# Navigation System Designs Based on Model Predictive and Sliding Mode Control for A Driverless Car's Trajectory Tracking

**Ngoc Dai Pham**
Lecturer
Department of Automotive Engineering
Faculty of Transportation Engineering, Ho Chi Minh City University of Technology (HCMUT) - Vietnam National University Ho Chi Minh City, 268 Ly Thuong Kiet Street
Dien Hong Ward, Ho Chi Minh City
Vietnam

*This study designs modern controllers, SMC and MPC, for vehicle motion control to ensure accurate trajectory tracking at the desired speed. Longitudinal motion is regulated via throttle and brake using a PD-FLC controller, while lateral motion is controlled through steering angle with SMC and MPC. The novelty of SMC lies in using Decoupled Algorithm, addressing a model where the steering input simultaneously affects translational dynamics and rotational dynamics, which is not widely applied in autonomous vehicles. The MPC novelty lies in using a precomputed adjustable coefficient matrix based on the receding horizon principle, simplifying design compared to continuous optimization during operation. Simulations in Matlab Simulink/Carsim under "Handling Course Left Edge" and "Double-Lane Change" showed that in Case 1, MPC achieved better performance metrics, with a 15% lower average distance error than SMC, while in Case 2, SMC outperformed MPC across all metrics, particularly in trajectory adherence, with 20% improvement.*

***Keywords:*** *Genetic Algorithm, Sliding-Mode Control, Model Predictive Control, Decoupled Algorithm, Carsim.*

## 1. INTRODUCTION

The process of automation is increasingly developing and becoming widespread across various fields, parti–cularly in transportation, with autonomous vehicles being a prime example. Autonomous vehicles are diverse, including ground-based vehicles (*AGVs*) [1,2], aerial vehicles (*UAVs*) [3,4], and underwater vehicles (*AUVs*) [5,6]. Among these, automobiles are one of the most common ground transportation modes and have attracted significant attention in the development of autonomous features. Research on self-driving cars began early and has been applied in practice [7,8]. This technology continues to advance rapidly due to the diverse real-world operating conditions and the growing emphasis on safety and stability to enhance human utility [9,10]. Autonomous vehicles are studied using control models for both lateral and longitudinal motion under a wide range of operating conditions [11–14]. Design evaluation methods are also diverse, ranging from simulation environments with specialized software such as Carsim to real-world testing [1,16].

In trajectory tracking control, vehicle control sys–tems must ensure sufficient traction to achieve the desired speed while maintaining the steering wheel angle to follow the intended path. Penglei Dai and colleagues [17] applied an *SMC*-based controller (Sliding-Mode Control) to manage the steering angle and an online-optimized *PID* controller using *PSO* to control the driving wheel torque in a 4×4 vehicle model Raghavendra's team [18] designed and experimentally evaluated an *SMC* controller with a Proportional–Derivative sliding surface for vehicle motion control, integrating *Fuzzy Logic* to fine-tune the sliding surface parameters based on error and error rate, enhancing system stability. Baosen Ma's group [19] proposed an *RITSMC* (Recursive Integral Terminal Sliding Mode Control) design method, combining the advantages of *RISM*, *TSM*, and optimization algorithms, demonstrating superior performance under various test conditions compared to conventional *SMC* and *ITSMC*. Fengxi Xie and colleagues developed an adaptive *SMC* capable of simultaneously controlling longitudinal and lateral ve–hicle motion, with parameters optimized using *PSO* and improved *GWO* algorithms [20]. Ping Hu's team pro–posed an *SMC* design with parameters adjusted via fuzzy logic to reduce chattering in longitudinal motion control of autonomous vehicles [21].

In addition to *SMC*, *MPC* (Model Predictive Cont–rol) and its variants are widely applied in autonomous vehicle control. Specifically, Jiechao Liu and colleagues implemented an *MPC* controller on a high-center-of-gravity autonomous vehicle to reach a target position as quickly as possible without a reference trajectory. The system allows the vehicle to generate its own trajectory by optimizing a spatial objective function while ensu–ring wheel-road adherence through steering angle cons–traints using a 14-DOF dynamic model [22]. Chuanyang Sun and colleagues applied an improved *MPC* with fuzzy logic support to ensure lateral motion control in both steady-state and transient conditions, demonstra–ting higher trajectory tracking performance compared to non-adaptive systems [23]. Young-Min Choi and Jahng-Hyon Park proposed a novel game-based coupling

Received: January 2026, Accepted: July 2026
Correspondence to: Ngoc Dai Pham, Faculty of Transportation Engineering, Ho Chi Minh City University of Technology, Ho Chi Minh City, Vietnam
E-mail: phamngocdai@hcmut.edu.vn
**doi: 10.5937/fme2603549P**

control method, which outperformed traditional *MPC* in maintaining lateral trajectory, passenger comfort, and vehicle stability [24]. Jianjun Hu's group integrated image processing to detect road paths as input for an *MPC* controller, combined with an *FLC*-based (Fuzzy Logic Control) regulator to limit the steering angle when yaw and yaw rate errors exceeded acceptable thresholds [25]. Chaoyong Zhang and colleagues designed an autonomous driving system for a *BYD* vehicle using a State Lattice-based trajectory model and *MPC* to navigate Double-Lane Change and fixed closed-loop trajectories at speeds of 40 and 60 km/h [26]. Fen Lin's team developed an adaptive *MPC* based on a 3-DOF vehicle dynamic model, adjusting for tire-road adhesion and vehicle speed for emergency lane-change scenarios, with performance evaluated in Carsim [27]. Changhee Kim's group designed a decision-making model to navigate around static obstacles and other vehicles using a 3-DOF MPC-based vehicle model [28]. Finally, Fitri Yakub's team designed an MPC to control vehicle body yaw torque, ensuring successful double-lane change trajectory tracking under high speed, slippery road conditions, and crosswind disturbances [29].

In addition to *SMC* and *MPC*-based controllers, *FLC* has also been widely applied in autonomous vehicle control. While *SMC* and *MPC* systems require a vehicle dynamic model to compute control inputs based on the vehicle's state [18, 19, 27, 28], *FLC* design does not require explicit equations describing control input evolution over time [30,31]. Neil Eugene Hodge and colleagues proposed a modular FLC-based trajectory control system, integrating one *FLC* with four modules for steering angle control and another *FLC* with three modules for speed control [30]. Subramanian V and colleagues designed a sensor fusion navigation system using an enhanced Kalman Filter combined with fuzzy logic, integrating data from machine vision, *LIDAR*, *IMU*, and speed sensors [31]. Bhakti Yudho and colleagues proposed a Type-2 *FLC* for lateral vehicle motion control, enabling trajectory tracking and obstacle avoidance, demonstrating superior performance compared to traditional *PID* controllers [32]. Thinh and Phuong employed 3D LiDAR technology for industrial autonomous vehicles, demonstrating superior performance compared with conventional 2D LiDAR systems [33].

The longitudinal vehicle speed is significantly influenced by lateral motion [34], requiring the driver to continuously adjust the throttle and brake pedals to maintain the desired speed. To capture this complex human behavior, previous studies have employed various control strategies, yet *PD-FLC* (Proportional Derivative) controllers, which can respond effectively to rapidly changing system states, have not been widely applied. While *SMC*-based lateral control methods are diverse, the use of a Decoupled Algorithm to simplify design and the incorporation of Hurwitz conditions to accurately calculate the correlation between control parameters have not been explored. *MPC* applications typically rely on continuous optimization over the control horizon, using the first computed value via *QP* (Quadratic Program), which complicates the design process. Moreover, systematic and efficient optimization of the state weighting matrices in the control signal has not been clearly addressed. Therefore, this study aims to contribute simplified *SMC* and *MPC* design methods for autonomous vehicles, capturing high correlations among control parameters to achieve improved operational performance. The main novelties and contributions of this research include:

1) A *PD-FLC* design method for longitudinal vehicle motion control, capable of effectively responding to rapid variations in vehicle speed state errors.

2) A simplified *SMC* design method using the Decoupled Algorithm, ensuring high accuracy in the correlation of sliding surface parameters based on Hurwitz conditions.

3) An *MPC* design method with control inputs directly determined according to the Receding Horizon Control principle, simplifying the computation process.

## 2. SIMULATION MODEL

### 2.1 OF planar model

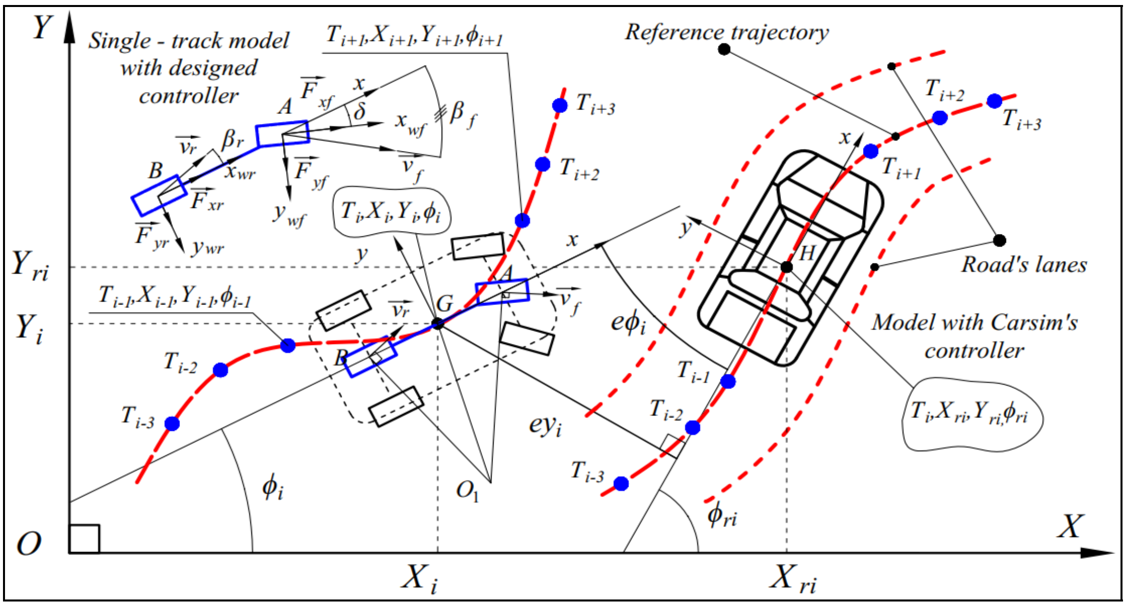


**Figure 1. 3-DOF vehicle dynamics model in the OXY Plane**

Many types of simulation models can be used to describe vehicle dynamics with different degrees of freedom (DOF), such as single-track models with 3 DOF, two-track models with 4 DOF, or full 6-DOF models [34]. This study adopts a single-track, three-degree-of-freedom (3-DOF) vehicle dynamics model in the *OXY* plane, which includes translational motions along the *X* and *Y* axes and rotation about the vertical axis. The overall analysis framework consists of two models: the controlled model used for controller design and implementation, and the reference model (with Carsim's controller). Both models are simulated within the Carsim environment and integrated with Matlab Simulink.

The controlled vehicle model includes steering wheel, throttle, and brake controllers, while the reference model only has throttle and brake control. Each vehicle model has its own coordinate system with the origin at the vehicle's center of gravity, denoted as *Gxy* for the controlled vehicle and *Hxy* for the reference vehicle. At each time step $T_i$, both the controlled and reference models are operated, and signals such as velocity, acceleration, and angular rate are recorded to compute the vehicle coordinates $X_i – X_{ri}$, $Y_i – Y_{ri}$, and heading angle $□_i – □_{ri}$. From these, the lateral distance $ey_i$ and heading deviation $e□_i$ between the controlled and reference vehicles are determined. The set of reference vehicle coordinates over the entire simulation period defines the desired trajectory that the controlled vehicle must follow.

Although roll motions around the *Gx* and *Hx* axes and pitch motions around the *Gy* and *Hy* axes affect vehicle behavior over time, the mathematical models for the designed controllers in this study are based on the 3-DOF model, which neglects these roll and pitch dynamics. However, the controller parameters are calibrated with the Carsim vehicle model, ensuring effective performance even in the presence of roll and pitch motions. Stability-related responses at the tire-road interface are represented using the built-in tire model provided by Carsim.

### 2.2 Mathematical model

The mathematical model describing the vehicle's lateral dynamics is established for the design of lateral motion controllers using *SMC* and *MPC*. The lateral forces exerted by the road on the front and rear wheels, $F_{yf}$ and $F_{yr}$, during vehicle steering are calculated based on the Pacejka tire model [34]. However, within the scope of this study, the Pacejka model is linearized for small tire slip angles as expressed in (1) [34]:

$$\begin{cases} F_{yf} = F_{zf}\mu_y\left(\alpha_f\right) \approx C_{\alpha f}\alpha_f, \alpha_f = \delta - \beta_f \le 10^o \\ F_{yr} = F_{zr}\mu_y\left(\alpha_r\right) \approx -C_{\alpha r}\alpha_r, \alpha_r = \beta_r \le 10^o \end{cases} \tag{1}$$

Considering the vehicle speeds at point $A – v_f$ and point $B – v_r$, we have:

$$\begin{cases} \vec{v}_f = \vec{v}_{A/O_1} = \vec{v}_{A/G} + \vec{v}_{G/O_1} \\ \vec{v}_r = \vec{v}_{B/O_1} = \vec{v}_{B/G} + \vec{v}_{G/O_1} \end{cases} \Rightarrow \begin{cases} v_{fx} = v_{rx} = \dot{x} \\ v_{fy} = a_1\dot{\phi} + \dot{y} \\ v_{ry} = -a_2\dot{\phi} + \dot{y} \end{cases} \tag{2}$$

Considering the vehicle acceleration at point *G*, we have:

$$\vec{a}_G = \vec{a}_{Gt} + \vec{a}_{Gn}$$

$$\begin{cases} a_{Gx} = \ddot{x} - \dfrac{v^2}{O_1G}cos\left(\dfrac{\pi}{2} - \beta\right) = \ddot{x} - \dfrac{v}{O_1G}.vsin\beta \\ \qquad = \ddot{x} - \dot{\phi}\dot{y} \\ a_{Gy} = \ddot{y} + \dfrac{v^2}{O_1G}sin\left(\dfrac{\pi}{2} - \beta\right) = \ddot{y} + \dfrac{v}{O_1G}.\dot{x}vcos\beta \\ \qquad = \ddot{y} + \dot{\phi}\dot{x} \end{cases} \tag{3}$$

With the force vectors at the front wheels $F_{xf}$ - $F_{yf}$ and rear wheels $F_{xr} - F_{yr}$, the dynamic equations describing the vehicle motion along the *Gx*, *Gy*, and vertical directions are formulated according to Newton's Second Law (4).

$$\begin{cases} \ddot{x} = \dfrac{1}{m}\left[-C_{\alpha f}\left(\delta - \arctan\dfrac{a_1\dot{\phi} + \dot{y}}{\dot{x}}\right)\sin\delta + F_{xf}\cos\delta + F_{xr}\right] + \dot{\phi}\dot{y} \\ \ddot{y} = \dfrac{1}{m}\left[C_{\alpha f}\left(\delta - \arctan\dfrac{a_1\dot{\phi} + \dot{y}}{\dot{x}}\right)\cos\delta + F_{xf}\sin\delta - C_{\alpha r}\arctan\dfrac{-a_2\dot{\phi} + \dot{y}}{\dot{x}}\right] - \dot{\phi}\dot{x} \\ \ddot{\phi} = \dfrac{1}{I_z}\left\{\left[C_{\alpha f}\left(\delta - \arctan\dfrac{a_1\dot{\phi} + \dot{y}}{\dot{x}}\right)\cos\delta + F_{xf}\sin\delta\right]a_1 + C_{\alpha r}\arctan\dfrac{-a_2\dot{\phi} + \dot{y}}{\dot{x}}a_2\right\} \end{cases} \tag{4}$$

The dynamic model (4) is linearized by considering the steering angle $\delta$ to be below 10°.

$$\begin{cases} \ddot{x} = \dfrac{1}{m}\sum F_x + \dot{\phi}\dot{y} \\ \ddot{y} = \dot{\phi}\dfrac{\left(-a_1C_{\alpha f} + a_2C_{\alpha r}\right)}{m\dot{x}} - \dot{y}\dfrac{\left(C_{\alpha f} + C_{\alpha r}\right)}{m\dot{x}} + \delta\dfrac{C_{\alpha f}}{m} - \dot{\phi}\dot{x} \\ \ddot{\phi} = \dot{\phi}\dfrac{\left(-a_1^2C_{\alpha f} - a_2^2C_{\alpha r}\right)}{I_z\dot{x}} - \dot{y}\dfrac{\left(a_1C_{\alpha f} - a_2C_{\alpha r}\right)}{I_z\dot{x}} + \delta\dfrac{a_1C_{\alpha f}}{I_z} \end{cases} \tag{5}$$

The vehicle coordinates in the *OXY* coordinate system are determined based on the integral of the vehicle's instantaneous velocity values $v_x$, $v_y$ along the *OX* and *OY* directions (6).

$$\begin{cases} \vec{v}_X = \vec{v}_{x/X} + \vec{v}_{y/X} \Rightarrow X = \displaystyle\int_0^t \left(\dot{x}\cos\phi - \dot{y}\sin\phi\right)dt \\ \vec{v}_Y = \vec{v}_{x/Y} + \vec{v}_{y/Y} \Rightarrow Y = \displaystyle\int_0^t \left(\dot{x}\sin\phi + \dot{y}\cos\phi\right)dt \end{cases} \tag{6}$$

The controllers are designed based on the optimi–zation of the distance error $ey$ and heading error $e$□. Ac–cording to the analysis diagram in Figure 1, these values are determined through the vehicle coordinates $X$, $Y$ and heading □ as in (7). $X$ and $Y$ denote the vehicle coor–dinates in the global $XOY$ reference frame, whereas $x$ and $y$ represent the instantaneous displacement states of the vehicle in the local $xGy$ coordinate frame.

$$\begin{cases} e\phi_i = \phi_i - \phi_{ri} \\ ey_i = \left(X_i - X_{ri}\right)\sin\phi_{ri} - \left(Y_i - Y_{ri}\right)\cos\phi_{ri} \end{cases} \tag{7}$$

Derivative of input signals:

$$\begin{cases} \dot{e}\phi_i = \dot{\phi}_i - \dot{\phi}_{ri} \\ \dot{e}y_i = \dot{x}\sin e_{\phi i} + \dot{y}\cos e_{\phi i} \approx \dot{x}e_{\phi i} + \dot{y} \end{cases} \tag{8}$$

### 2.3 Test cases' set up with Carsim software

The study designs controllers to ensure the vehicle fol–lows the desired speed and trajectory under operational scenarios including: starting on a long and complex trajectory from 0 km/h and maintaining stability at 40 km/h, Figure 2, which represents the permissible speed on urban roads in Ho Chi Minh City, Vietnam; and the "*Double-Lane Change*" scenario at 120 km/h, Figure 3, which corresponds to the maximum allowable speed on highways in Vietnam. These scenarios assume good road conditions with a static friction coefficient $\mu$=0.9. The controllers are implemented in Matlab Simulink and interact with the Carsim vehicle model. Further–more, the controller parameters are primarily optimized to handle the first scenario while their obstacle avoi–dance capa–bility at high speed is verified using the second scenario.

***Case 1: Handling course left edge***

The road is 2,328 m long within a test area of 470 m in length and 360 m in width, with 2 lanes, Figure 2a. The road elevation relative to the starting point varies continuously, with a maximum height of 5.2 m and a minimum of -2.5 m, Figure 2b.

**a. Route's map**

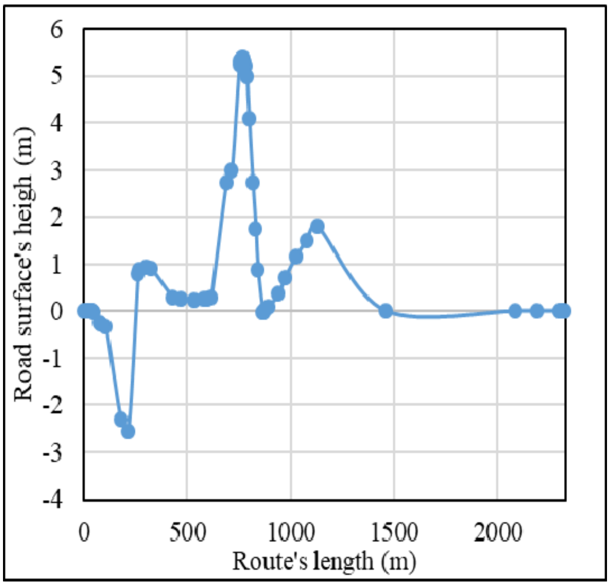


**b. Route's heigh**

**Figure 2. Long route at constant speed 40 (km/h)**

In Carsim, the environment and test model are set up in the "*Road X-Y-Z edges*" procedure, with the trajectory defined in the "*Reference Path: X-Y Coordinates of Path*" and "*Handling Course Left Edge*" modules. This trajectory is suitable for test scenarios with diverse curves and repetitive patterns. In this Carsim module, the user configures "*Driver Controls*" with the throttle mode set to "*Do not specify speed control here*" and the brake mode set to "*No linked*" allowing direct input of throttle and brake positions from the *PD-FLC* controller.

***Case 2: Double-lane change***

The lane-change section is 75 m long, with a distance of 3.5 m between the two lanes, and the vehicle speed at the start of the lane change is 120 km/h, Figure 3. In Carsim, the environment and test model are set up in the "*DLC @ 120 km/h*" procedure, with the trajectory defined in the "*Steering: Driver Path Follower*" and "*Double-Lane Change (Quick Start)*" modules. In this scenario, the vehicle speed is maintained by default in Carsim, and only the steering angle controller is evaluated.

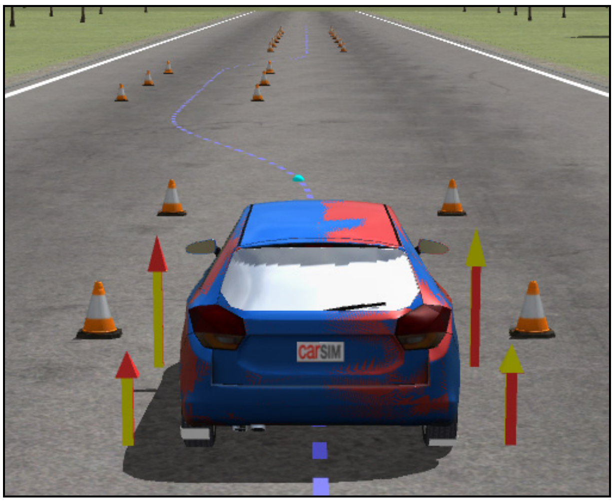


**Figure 3. Double-lane change at 120 (km/h)**

In this Carsim module for Case 2, the user configures "*Driver Controls*" with the throttle mode set to "*Constant target speed – 120 km/h*" In this case, the *PD-FLC* is not applied for vehicle speed control; the Carsim controller is used instead. Only the steering angle controllers, *SMC* and *MPC*, are employed.

The specifications of the test tracks, such as total travel length, lane spacing, slope, and friction coefficient, are set according to Carsim's standard testing conditions. Only the auxiliary *ABS* system is activated during the test scenarios, with operating parameters set to Carsim's default values.

## 3. CONTROLLERS' DESIGN

### 3.1. Longitudinal motion

The vehicle's longitudinal motion (speed) is controlled by a *PD-FLC* (proportional–derivative fuzzy logic cont–roller). The vehicle speed is regulated via throttle and brake positions in the "*Driver Control*" section of the "*Road X-Y-Z edges*" procedure. The control signal is the error between the desired vehicle speed $v_{ref}$=40 km/h and the actual vehicle speed $v_{real}$. However, the value applied for *PD-FLC* optimization according to the *ITAE* standard [35, 36] is the position error *ey* between the controlled vehicle and the reference vehicle in Carsim.

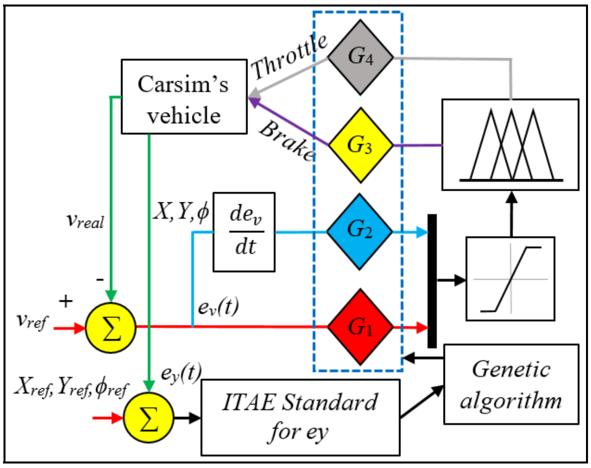


Figure 4. PD FLC's diagram

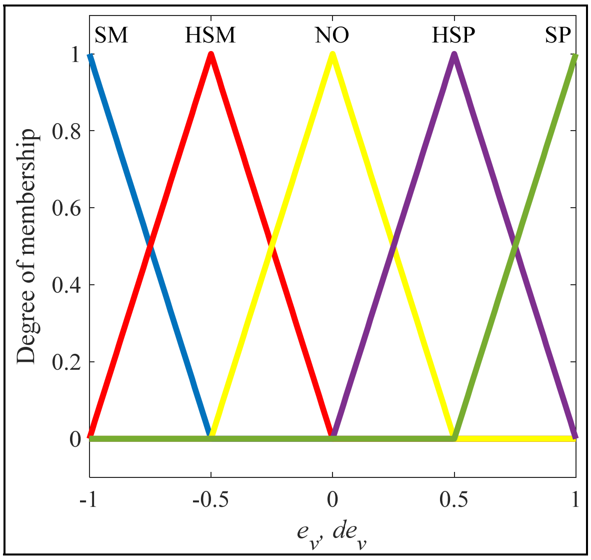


a. Membership function of $e_v$, $de_v$

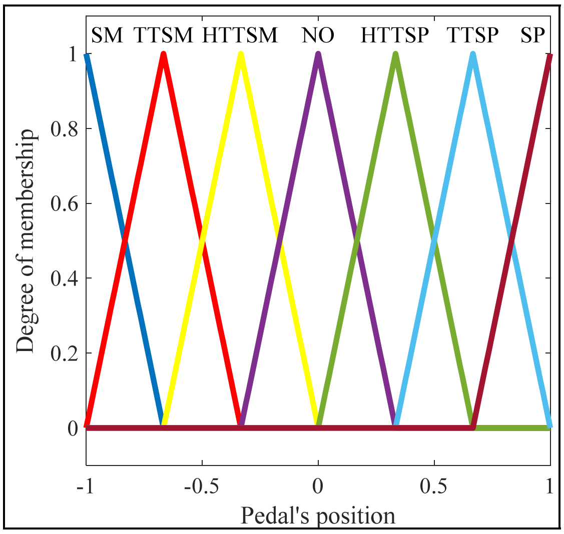


b. Membership function of pedal's position

Figure 5. Membership function for ev, dev, pedal's position

The *ey* value is calculated based on the controlled vehicle data $X$, $Y$, □ and the reference vehicle data $X_{ref}$, $Y_{ref}$, □$_{ref}$ according to equation (7). Applying *ey* for *ITAE* instead of $e_v$ is justified because when the vehicle fol–lows the desired trajectory accurately, the vehicle speed naturally reaches the desired value. The *PD-FLC* cont–roller parameters are tuned for optimal performance, including $G_1$, $G_2$, $G_3$, $G_4$. These parameters are deter–mined by *GA* based on the minimum *ITAE* obtained.

The study applies a fuzzy logic controller with trian–gular membership functions for both input and output signals. The input signals $e_v$ and $de_v$ have five member–ship levels: "*SM – Significant Minus*", "*HSM – Half Significant Minus*", "*NO – Non*", "*SP – Significant Plus*", and "*HSP – Half Significant Plus*". The output signals, representing throttle and brake positions, have seven mem–bership levels: "*SM – Significant Minus*", "*TTSM – Two-Third Significant Minus*", "*HTTSM – Half of Two-Third Significant Minus*", "*NO – Non*", "*SP – Significant Plus*", "*TTSP – Two-Third Significant Plus*", and "*HTTSP – Half of Two-Third Significant Plus*". The relationships between the input and output membership functions are defined by the design rules presented in Table 1. These re–lationships are visually represented in a 3D graph, Figure 6.

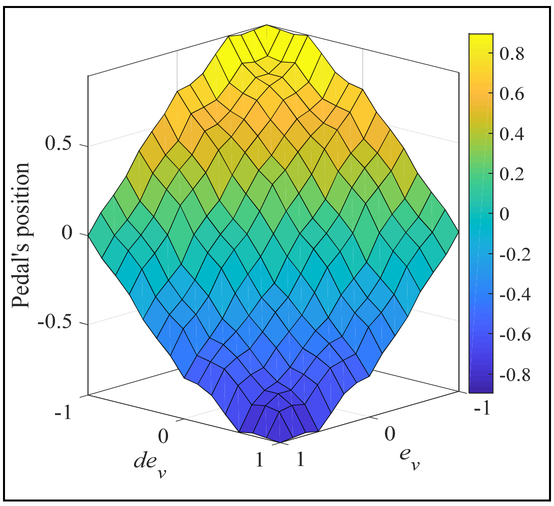


Figure 6. Control surface

**Table 1. PD - FLC rules**

| Pedal's position | | Error of velocity ($e_v$) | | | | |
|---|---|---|---|---|---|---|
| | | **SM** | **HSM** | **NO** | **HSP** | **SP** |
| $de_v$ | **SM** | SP | SP | TTSP | HTTSP | NO |
| | **HSM** | SP | TTSP | HTTSP | NO | HTTSM |
| | **NO** | TTSP | HTTSP | NO | HTTSM | TTSM |
| | **HSP** | HTTSP | NO | HTTSM | TTSM | SM |
| | **SP** | NO | HTTSM | TTSM | SM | SM |

## 3.2 Lateral motion

### 3.2.1. Model predictive controller – *MPC*

The *MPC* controller for steering angle control of the front wheels is designed based on the 3-DOF dynamic model according to (5) and (8). The steps for designing the *MPC* controller follow the procedure below [37].

Establish the state variable matrix of the model $X$ and transform equations (5) and (8) into the general form with $X$ as in (9).

$$X = \begin{bmatrix} x_1 & x_2 & x_3 & x_4 & x_5 & x_6 & x_7 & x_8 \end{bmatrix}^T$$

With:

$$x_1 = y, x_2 = \dot{y}, x_3 = \phi, x_4 = \dot{\phi},$$
$$x_5 = ey, x_6 = \dot{e}y, x_7 = e\phi, x_8 = \dot{e}\phi$$

Therefore:

$$\dot{X} = AX + BU + Dd$$

$$\begin{bmatrix} \dot{x}_1 \\ \dot{x}_2 \\ \dot{x}_3 \\ \dot{x}_4 \\ \dot{x}_5 \\ \dot{x}_6 \\ \dot{x}_7 \\ \dot{x}_8 \end{bmatrix} = \begin{bmatrix} 0 & 1 & 0 & 0 & 0 & 0 & 0 & 0 \\ 0 & \frac{-C_{\alpha f} - C_{\alpha r}}{m\dot{x}} & 0 & \frac{-a_1 C_{\alpha f} + a_2 C_{\alpha r}}{m\dot{x}} - \dot{x} & 0 & 0 & 0 & 0 \\ 0 & 0 & 0 & 1 & 0 & 0 & 0 & 0 \\ 0 & \frac{-a_1 C_{\alpha f} + a_2 C_{\alpha r}}{I_z \dot{x}} & 0 & \frac{-a_1^2 C_{\alpha f} - a_2^2 C_{\alpha r}}{I_z \dot{x}} & 0 & 0 & 0 & 0 \\ 0 & 0 & 0 & 0 & 0 & 1 & 0 & 0 \\ 0 & \frac{-C_{\alpha f} - C_{\alpha r}}{m\dot{x}} & 0 & \frac{-a_1 C_{\alpha f} + a_2 C_{\alpha r}}{m\dot{x}} - \dot{x} & 0 & 0 & 0 & \dot{x} \\ 0 & 0 & 0 & 0 & 0 & 0 & 0 & 1 \\ 0 & \frac{-a_1 C_{\alpha f} + a_2 C_{\alpha r}}{I_z \dot{x}} & 0 & \frac{-a_1^2 C_{\alpha f} - a_2^2 C_{\alpha r}}{I_z \dot{x}} & 0 & 0 & 0 & 0 \end{bmatrix} \begin{bmatrix} x_1 \\ x_2 \\ x_3 \\ x_4 \\ x_5 \\ x_6 \\ x_7 \\ x_8 \end{bmatrix} + \begin{bmatrix} 0 \\ \frac{C_{\alpha f}}{m} \\ 0 \\ \frac{a_1 C_{\alpha f}}{I_z} \\ 0 \\ \frac{C_{\alpha f}}{m} \\ 0 \\ \frac{a_1 C_{\alpha f}}{I_z} \end{bmatrix} \delta + \begin{bmatrix} 0 \\ 0 \\ 0 \\ 0 \\ 0 \\ 0 \\ 0 \\ -1 \end{bmatrix} \ddot{\phi}_r \tag{9}$$

Establish the general discrete-time dynamic model by discretizing (9) using Matlab. The general discrete equation is given in (10).

$$\begin{cases} x_m(k+1) = A_m x_m(k) + B_m u(k) + D_m d(k) \\ y(k) = C_m x_m(k) \end{cases} \tag{10}$$

Transform the discrete-time model into the "*Argu–ment*" form. We have:

$$\bullet \begin{cases} \circ x_m(k+1) - x_m(k) = A_m\left[x_m(k) - x_m(k-1)\right] + ... \\ B_m\left[u(k) - u(k-1)\right] + D_m\left[d(k) - d(k-1)\right] \\ \circ y(k+1) - y(k) = C_m\left[x_m(k+1) - x_m(k)\right] \end{cases}$$

$$\bullet \begin{cases} \Delta x_m(k+1) = x_m(k+1) - x_m(k) \\ \Delta x_m(k) = x_m(k) - x_m(k-1) \\ \Delta u(k) = u(k) - u(k-1) \\ \Delta d(k) = d(k) - d(k-1) \end{cases} \tag{11}$$

Therefore:

$$\begin{cases} \bullet \Delta x_m(k+1) = A_m \Delta x_m(k) + B_m \Delta u(k) + ... \\ D_m \Delta d(k) \\ \bullet y(k+1) = C_m A_m \Delta x_m(k) + C_m B_m \Delta u(k) + ... \\ C_m D_m \Delta d(k) + y(k) \end{cases} \tag{12}$$

Control form:

$$\begin{cases} \bullet \begin{bmatrix} \Delta x_m(k+1) \\ y(k+1) \end{bmatrix} = \begin{bmatrix} A_m & o_m^T \\ C_m A_m & 1 \end{bmatrix} \begin{bmatrix} \Delta x_m(k) \\ y(k) \end{bmatrix} + ... \\ \begin{bmatrix} B_m \\ C_m B_m \end{bmatrix} \Delta u(k) + \begin{bmatrix} D_m \\ C_m D_m \end{bmatrix} \Delta d(k) \\ \bullet y(k) = \begin{bmatrix} o_m & 1 \end{bmatrix} \begin{bmatrix} \Delta x_m(k) \\ y(k) \end{bmatrix} \end{cases} \tag{13}$$

$$\Leftrightarrow \begin{cases} \tilde{x}(k+1) = A\tilde{x}(k) + B\Delta u(k) + D\Delta d(k) \\ \tilde{y}(k) = C\tilde{x}(k) \end{cases}$$

Consider over the domain of control horizon $N_c$ and prediction horizon $N_p$:

$$\begin{aligned} &\bullet \tilde{x}(k_i+1 \mid k_i) = A\tilde{x}(k_i) + B\Delta u(k_i) + D\Delta d(k_i) \\ &\bullet \tilde{x}(k_i+2 \mid k_i) = A^2\tilde{x}(k_i) + AB\Delta u(k_i) + B\Delta u(k_i+1) + ... \\ &AD\Delta d(k_i) + D\Delta d(k_i+1) \\ &\bullet \tilde{x}(k_i+3 \mid k_i) = A^3\tilde{x}(k_i) + A^2B\Delta u(k_i) + AB\Delta u(k_i+1) + ... \\ &B\Delta u(k_i+2) + A^2D\Delta d(k_i) + AD\Delta d(k_i+1) + D\Delta d(k_i+2) \\ &\vdots \\ &\bullet \tilde{x}(k_i+N_p \mid k_i) = A^{N_p}\tilde{x}(k_i) + A^{N_p-1}B\Delta u(k_i) + ... \\ &+A^{N_p-N_c}B\Delta u(k_i+N_c-1) + A^{N_p-1}D\Delta d(k_i) + ... \\ &+D\Delta d(k_i+N_p-1) \end{aligned} \tag{14}$$

Therefore:

$$\begin{aligned}
&\bullet y(k_i+1|k_i)=CAx(k_i)+CB\Delta u(k_i)+CD\Delta d(k_i)\\
&\bullet y(k_i+2|k_i)=CA^2x(k_i)+CAB\Delta u(k_i)+CB\Delta u(k_i+1)+...\\
&CAD\Delta d(k_i)+CD\Delta d(k_i+1)\\
&\bullet y(k_i+3|k_i)=CA^3x(k_i)+CA^2B\Delta u(k_i)+CAB\Delta u(k_i+1)+...\\
&CB\Delta u(k_i+2)+CA^2D\Delta d(k_i)+CAD\Delta d(k_i+1)+CD\Delta d(k_i+2)\\
&\vdots\\
&\bullet y(k_i+N_p|k_i)=CA^{N_p}x(k_i)+CA^{N_p-1}B\Delta u(k_i)+...\\
&+CA^{N_p-N_c}B\Delta u(k_i+N_c-1)+CA^{N_p-1}D\Delta d(k_i)+...\\
&+CD\Delta d(k_i+N_p-1)
\end{aligned} \tag{15}$$

Set:

$$\begin{cases}
Y=\left[y(k_i+1|k_i) \quad y(k_i+2|k_i) \quad \dots \quad y(k_i+N_p|k_i)\right]^T\\
\Delta U=\left[\Delta u(k_i) \quad \Delta u(k_i+1) \quad \dots \quad \Delta u(k_i+N_c-1)\right]^T\\
\Delta D=\left[\Delta d(k_i) \quad \Delta d(k_i+1) \quad \dots \quad \Delta d(k_i+N_p-1)\right]^T
\end{cases} \tag{16}$$

Set:

$$Y = Fx(k_i) + \Phi\Delta U + \tau\Delta D \tag{17}$$

With:

$$F_{N_p\times 1}=\begin{bmatrix} CA & CA^2 & CA^3 & CA^4 & \dots & CA^{N_p}\end{bmatrix}^T$$

$$\Phi_{N_p\times N_c}=\begin{bmatrix}
CB & 0 & 0 & \dots & 0\\
CAB & CB & 0 & \dots & 0\\
CA^2B & CAB & CB & \dots & 0\\
CA^3B & CA^2B & CAB & \dots & 0\\
CA^4B & CA^3B & CA^2B & \dots & 0\\
\vdots & \vdots & \vdots & \vdots & \vdots\\
CA^{N_p-1}B & CA^{N_p-2}B & CA^{N_p-3}B & \dots & CA^{N_p-N_c}B
\end{bmatrix}$$

$$\tau_{N_p\times N_p}=\begin{bmatrix}
CD & 0 & 0 & \dots & 0\\
CAD & CD & 0 & \dots & 0\\
CA^2D & CAD & CD & \dots & 0\\
CA^3D & CA^2D & CAD & \dots & 0\\
CA^4D & CA^3D & CA^2D & \dots & 0\\
\vdots & \vdots & \vdots & \vdots & \vdots\\
CA^{N_p-1}D & CA^{N_p-2}D & CA^{N_p-3}D & \dots & CA^{N_p-N_p}D
\end{bmatrix}$$

Establish the quadratic objective function $J$ of the state variable errors and control input changes $\Delta U$ with weighting matrices $W_1$, $W_2$ according to (18).

$$\begin{aligned}
J &= (R_S-Y)^T W_1 (R_S-Y)+\Delta U^T W_2 \Delta U\\
&=\left(R_S-Fx(k_i)-\Phi\Delta U-\tau\Delta D\right)^T W_1\left(R_S-Fx(k_i)-\Phi\Delta U-\tau\Delta D\right)+\Delta U^T W_2\Delta U
\end{aligned} \tag{18}$$

$$W_{1(N_p\times N_p)}=\begin{bmatrix}
I_w & 0 & 0 & \dots & 0\\
0 & I_w & 0 & \dots & 0\\
0 & 0 & I_w & \dots & 0\\
\vdots & \vdots & \vdots & \ddots & \vdots\\
0 & 0 & 0 & \dots & I_w
\end{bmatrix}$$

$$I_{w(12\times 12)}=\begin{bmatrix}
w_1 & 0 & 0 & \dots & 0\\
0 & w_2 & 0 & \dots & 0\\
0 & 0 & w_3 & \dots & 0\\
\vdots & \vdots & \vdots & \ddots & \vdots\\
0 & 0 & 0 & \dots & w_{12}
\end{bmatrix},$$

$$W_{2(N_c\times N_c)}=\begin{bmatrix}
w & 0 & 0 & \dots & 0\\
0 & w & 0 & \dots & 0\\
0 & 0 & w & \dots & 0\\
\vdots & \vdots & \vdots & \ddots & \vdots\\
0 & 0 & 0 & \dots & w
\end{bmatrix}$$

Determine the value of $\Delta U$ that minimizes $J$ by taking the derivative of the quadratic equation of $J$ with respect to $\Delta U$ (19).

$$\begin{aligned}
&\frac{\partial J}{\partial \Delta U}=2\Delta U\left(\Phi^T W_1\Phi+W_2\right)-2\Phi^T W_1\left(R_S-Fx(k_i)\right)...\\
&+2\Phi^T W_1\tau\Delta D
\end{aligned} \tag{19}$$

$J$ reaches its minimum with the value of $\Delta U$ determined according to (20).

$$\begin{aligned}
&\frac{\partial J}{\partial \Delta U}=0\\
&\Rightarrow \Delta U=\left(\Phi^T W_1\Phi+W_2\right)^{-1}\Phi^T W_1\left(R_S-Fx(k_i)-\tau\Delta D\right)
\end{aligned} \tag{20}$$

### 3.2.2. Decoupled sliding-mode controller – *SMC*

Unlike the *MPC*, where the system model must integ–rate the influence of all state variables into a single control signal model, the *SMC* model is simpler, as it only varies according to the state variables that need to be stabilized, namely *ey* and *e*□. The *SMC* controller is designed using the "*Decoupled Algorithm*" (*DA*). *DA* addresses the situation where the system control input $\delta$ directly affects multiple dynamic equations simultane–ously according to (21) [38]. Accordingly, the *DA* method transforms the system of equations (21) into a new system as in (23), in which only one equation in–volves $\delta$. This process simplifies and improves the efficiency of establishing the control signal model $\delta(t)$ as in (31).

$$\begin{cases}
\ddot{e}y = f_1\left(\dot{e}\varepsilon, \dot{y}, \dot{\phi}\right)+g_1\left(e\phi\right)\delta\\
\ddot{e}\phi = f_2\left(\dot{e}\phi, \dot{y}, \dot{\phi}\right)+g_2\left(e\phi\right)\delta+d\left(\ddot{\phi}_r\right)
\end{cases} \tag{21}$$

where, $f_1$, $f_2$, $g_1$, $g_2$, $d$ can be calculated as (11).

$$\begin{cases} f_1 = \dot{x}\dot{e}\phi + \dfrac{1}{m\dot{x}}\left(-a_1C_{\alpha f} + a_2C_{\alpha r}\right)\dot{\phi}... \\ -\dfrac{1}{m\dot{x}}\left(C_{\alpha f} + C_{\alpha r}\right)\dot{y} - \dot{x}\dot{\phi} \\ f_2 = \dfrac{1}{I_z\dot{x}}\left(-a_1^2C_{\alpha f} - a_2^2C_{\alpha r}\right)\dot{\phi}... \\ -\dfrac{1}{I_z\dot{x}}\left(a_1C_{\alpha f} - a_2C_{\alpha r}\right)\dot{y} \\ g_1 = \dfrac{1}{m}C_{\alpha f}, g_2 = \dfrac{1}{I_z}a_1C_{\alpha f} \\ d = -\ddot{\phi}_r \end{cases} \tag{22}$$

Set:

$$\begin{cases} x_1 = ey - \dfrac{I_z}{ma_1}e\phi \\ x_2 = \dot{e}y - \dfrac{I_z}{ma_1}\dot{e}\phi \\ x_3 = e\phi \\ x_4 = \dot{e}\phi \end{cases} \tag{23}$$

Therefore:

$$\begin{cases} \dot{x}_1 = x_2 \\ \dot{x}_2 = \left(\dot{x} + f_3 + \dfrac{I_z}{ma_1}f_4\right)x_4 + f_4x_2 - \dot{x}f_4x_3 + f_3\dot{\phi}_r.... \\ +\dfrac{I_z}{ma_1}\ddot{\phi}_r \\ \dot{x}_3 = x_4 \\ \dot{x}_4 = -\ddot{\phi}_r + \dfrac{1}{I_z\dot{x}}\left(-a_1^2C_{\alpha f} - a_2^2C_{\alpha r}\right)\dot{\phi}_r... \\ -\dfrac{a_1C_{\alpha f} - a_2C_{\alpha r}}{I_z\dot{x}}x_2 + \dfrac{a_1C_{\alpha f} - a_2C_{\alpha r}}{I_z}x_3... \\ +\dfrac{ma_1\left(-a_1^2C_{\alpha f} - a_2^2C_{\alpha r}\right) - I_z\left(a_1C_{\alpha f} - a_2C_{\alpha r}\right)}{I_z\dot{x}ma_1}x_4... \\ +\dfrac{1}{I_z}a_1C_{\alpha f}\delta \end{cases} \tag{24}$$

Set:

$$\begin{cases} f_3 = \dfrac{a_2C_{\alpha r}l - ma_1\dot{x}^2}{ma_1\dot{x}} \\ f_4 = -\dfrac{C_{\alpha r}l}{ma_1\dot{x}} \end{cases} \tag{25}$$

Set:

$$\begin{cases} \mu_1 = x_4 \\ \mu_2 = \begin{bmatrix} x_1 & x_2 & x_3 \end{bmatrix}^T \\ C = \begin{bmatrix} c_1 & c_2 & c_3 \end{bmatrix} \end{cases} \tag{26}$$

Sliding surface:

$$\sigma = \mu_1 - C\mu_2 = x_4 - c_1x_1 - c_2x_2 - c_3x_3 \tag{27}$$

Derive sliding surface:

$$\begin{aligned} \dot{\sigma} &= \dot{\mu}_1 - C\dot{\mu}_2 \\ &= -\ddot{\phi}_r\left(1 + \frac{c_2I_z}{ma_1}\right) + \dot{\phi}_r f_5 + \left(f_6 - c_1\right)x_2 - \dot{x}f_6x_3... \\ &+\left(f_5 + \frac{I_zf_6}{ma_1} - c_2\dot{x} - c_3\right)x_4 + \frac{a_1C_{\alpha f}}{I_z}\delta \end{aligned} \tag{28}$$

Set:

$$\begin{cases} f_5 = \dfrac{-a_1^2C_{\alpha f} - a_2^2C_{\alpha r}}{I_z\dot{x}} - \dfrac{c_2a_2C_{\alpha r}l - c_2ma_1\dot{x}^2}{ma_1\dot{x}} \\ f_6 = \dfrac{-a_1C_{\alpha f} + a_2C_{\alpha r}}{I_z\dot{x}} + \dfrac{c_2C_{\alpha r}l}{ma_1\dot{x}} \end{cases} \tag{29}$$

According to quasi-sliding mode design with satu– ration function:

$$\begin{cases} \dot{\sigma} = -\eta sat\left(\sigma\right) \\ sat\left(\sigma\right) = \begin{cases} 1, if\, \sigma > \Delta \\ \dfrac{\sigma}{\Delta}, if\, \left|\sigma\right| \le \Delta \\ -1, if\, \sigma < -\Delta \end{cases} \end{cases} \tag{30}$$

Therefore:

$$\delta = \frac{I_z}{a_1C_{\alpha f}}\begin{bmatrix} -\eta sat\left(\sigma\right) + \ddot{\phi}_r\left(1 + \dfrac{c_2I_z}{ma_1}\right) - \left(x_4 + \dot{\phi}_r\right)f_5... \\ -\left(x_2 - \dot{x}x_3 + \dfrac{I_z}{ma_1}x_4\right)f_6 + c_1x_2 + c_2\dot{x}x_4 + c_3x_4 \end{bmatrix} \tag{31}$$

Design the Lyapunov function as (35):

$$V = \frac{1}{2}\sigma^2 \tag{32}$$

Then:

$$\dot{V} = \sigma\dot{\sigma} = -\eta\,\text{sgn}(\sigma)\sigma \le 0 \tag{33}$$

From $\sigma\dot{\sigma} \le 0$ , under controller (38), the system can reach and thereafter stay on the manifold σ = 0 in infinite time $t_s$ (s). On the manifold we have:

$$\sigma = \mu_1 - C\mu_2 = 0 \Rightarrow \mu_1 = C\mu_2 \tag{34}$$

After $t_s$ (s),

$$\begin{cases} \dot{\mu}_2 = \begin{bmatrix} \dot{x}_1 \\ \dot{x}_2 \\ \dot{x}_3 \end{bmatrix} = \begin{bmatrix} x_2 \\ x_1c_1G + x_2\left(c_2G + f_4\right) + x_3\left(c_3G - \dot{x}f_4\right)... \\ +\dfrac{I_z}{ma_1}\ddot{\phi}_r + f_3\dot{\phi}_r \\ c_1x_1 + c_2x_2 + c_3x_3 \end{bmatrix} \\ G = \dot{x} + f_3 + \dfrac{I_z}{ma_1}f_4 \end{cases} \tag{35}$$

Set:

$$\dot{\mu}_2 = A_1\mu_1 + A_2\mu_2 + U = \left(A_1 C + A_2\right)\mu_2 + U$$
$$= A\mu_2 + U \quad (36)$$
$$= A\begin{bmatrix} x_1 \\ x_2 \\ x_3 \end{bmatrix} + U$$

$$A_1 = \begin{bmatrix} 0 & 0 & 1 \end{bmatrix}^T, C = \begin{bmatrix} c_1 & c_2 & c_3 \end{bmatrix},$$

$$A_2 = \begin{bmatrix} 0 & 1 & 0 \\ c_1 G & f_4 + c_2 G & -\dot{x} f_4 + c_3 G \\ 0 & 0 & 0 \end{bmatrix}, U = \begin{bmatrix} 0 \\ f_3\dot{\phi}_r + \frac{I_z}{m a_1}\ddot{\phi}_r \\ 0 \end{bmatrix}$$

$$\Rightarrow A = \begin{bmatrix} 0 & 1 & 0 \\ c_1 G & f_4 + c_2 G & -\dot{x} f_4 + c_3 G \\ c_1 & c_2 & c_3 \end{bmatrix}$$

To guaranteed $\mu_2$ become 0, $A$ should be Hurwitz. The poles of $A$ can be designed as:

$$\left|sI - A\right| = \begin{vmatrix} s & -1 & 0 \\ -c_1 G & s - f_4 - c_2 G & \dot{x} f_4 - c_3 G \\ -c_1 & -c_2 & s - c_3 \end{vmatrix}$$
$$= s^3 - s^2\left(c_3 + f_4 + c_2 G\right) + s\left(c_3 f_4 + c_2 \dot{x} f_4 - c_1 G\right) + c_1 \dot{x} f_4 \quad (37)$$
$$= 0$$

We have:

$$\left(s + p\right)^3 = s^3 + 3ps^2 + 3p^2 s + p^3 = 0, p > 0 \quad (38)$$

With (37), (38), we have (39):

$$\begin{cases} c_1 = \dfrac{p^3}{\dot{x} f_4} \\ c_2 = \dfrac{3p^2 + c_1 G + 3p f_4 + f_4^2}{f_4\left(\dot{x} - G\right)} \\ c_3 = -3p - f_4 - c_2 G \end{cases} \quad (39)$$

## 4. GENETIC ALGORITHM – *GA*

The genetic algorithm is used in this study to determine the optimal parameters for the *PD-FLC*, *SMC*, and *MPC* controllers. The *ITAE*-based objective function $J_{ITAE}$ according to the *ITAE* standard [35, 36] is selected (40) and optimized to identify the corresponding parameter values for the *PD-FLC*, *SMC*, and *MPC*. It should be noted that in this objective function, the distance error parameter *ey* is calculated according to equation (7) rather than (8).

$$J_{ITAE} = \int_0^{+\infty} t\left|\left[X(t) - X_r(t)\right]\sin\phi_{ri} - \left[Y(t) - Y_r(t)\right]\cos\phi_{ri}\right| dt \quad (40)$$

The constraints of the algorithm include ensuring that all wheels remain in contact with the road ($F_{zi}$>0) and that the maximum lateral acceleration *ay* along the *Gy* axis at any time does not exceed 8.83 m/s². Addi–tionally, the study evaluates the impact of the control process on the overall passenger perception according to ISO 2631:1-1997 [39], using the total acceleration $a_v$ across all three axes *Gx*, *Gy*, and *Gz*.

$$a_v = \left(k_x^2 a_{Wx}^2 + k_y^2 a_{Wy}^2 + k_z^2 a_{Wz}^2\right)^{1/2} \quad (41)$$

$$a_W = \sqrt{\frac{1}{T}\int_0^T a_w^2(t)\, dt} \quad (42)$$

$$a_w(t) = \sqrt{\sum_i \left(w_i a_i(t)\right)^2} \quad (43)$$

$$a_i(t) = \sqrt{\frac{1}{N}\sum_{j=1}^{N} a_j^2} = \sqrt{\frac{a_1^2 + a_2^2 + \ldots + a_N^2}{N}} \quad (44)$$

A step-by-step breakdown on controller optimization [40]:

**Step 1:** Define the system's technical parameters to be searched and the fitness function to be optimized

- The technical parameters of *PD–FLC*, *SMC* and *MPC* to be determined are in Table 3.
- The objective function is $J_{ITAE}$ calculated as (40).

**Step 2:** Choose the Genetic Algorithm's technical para–meters and create initial values of searched paremeters

- The population's size (number of individuals), the generation N as well as the indexes of crossover, mutation are chosen as in Table 3.
- Randomly initialize the searched parameters' values of each individual.

**Step 3:** Calculate the fitness function value $J_{ITAE}$ for each individual with the chosen system's technical parameters

**Step 4:** Select the individuals as parents with rank-based selection method

**Step 5:** Create mutation by applying small random changes to offspring

**Step 6:** Repeat this process N times and get the results

In this study, the total number of variables to be determined is large, ranging from 7 (*PD-FLC*, *SMC*) to 12 variables (*MPC*), so the population size and the number of generations for crossover also need to be correspondingly large. The selected parameters are summarized in Table 2.

**Table 2. Parameters' search region**

| Value | *GA-SMC* | *GA-MPC* |
|---|---|---|
| Variables' name | *p*, *η*, *Δ*, $G_1$, $G_2$, $G_3$, $G_4$ | $w_1$, $w_2$, $w_3$,...$w_{12}$ |
| Generation | 100 | 200 |
| Population size | 10 | 20 |
| Crossover | 0.8 | 0.8 |
| Mutation | 0.1 | 0.1 |
| Fitness function | $J_{ITAE}$ | $J_{ITAE}$ |

| *GA-SMC*'s search region | | |
|---|---|---|
| Value | Lower bound | Upper bound |
| *p* | 0.01 | 0.1 |
| *η* | 500 | 1000 |
| *Δ* | 0.1 | 1 |
| $G_1$ | 0.1 | 5 |

| | | |
|---|---|---|
| $G_2$ | 0.01 | 0.1 |
| $G_3$ | 0.1 | 1 |
| $G_4$ | 1 | 300 |
| *GA-MPC*'s search region | | |
| Value | Lower bound | Upper bound |
| $w_{1\ldots12}$ | 0 | 1 |

## 5. RESULTS AND DISCUSSIONS

The results of the controller parameter optimization process are summarized in Table 3.

**Table 3. Optimal parameters summary**

| GA's search results | | | |
|---|---|---|---|
| Value | *GA-SMC* | Value | *GA-MPC* |
| $P$ | 0.0445 | $w_1$ | 0.0015 |
| $H$ | 973.4083 | $w_2$ | 0.3626 |
| $\Delta$ | 0.6124 | $w_3$ | 0.0152 |
| $G_1$ | 1.3187 | $w_4$ | 0.6179 |
| $G_2$ | 0.1000 | $w_5$ | 0.2788 |
| $G_3$ | 0.5225 | $w_6$ | 0.2453 |
| $G_4$ | 161.5577 | $w_7$ | 0.1527 |
| -- | -- | $w_8$ | 0.8068 |
| -- | -- | $w_9$ | 0.0012 |
| -- | -- | $w_{10}$ | 0.0207 |
| -- | -- | $w_{11}$ | 0.7908 |
| -- | -- | $w_{12}$ | 0.7904 |

### 5.1 Case 1

The study evaluates the performance of the controllers in Case 1 according to the criteria of the root mean square (RMS) of the distance error *ey*, heading error *e*□, lateral acceleration *ay*, and vehicle body roll angle *θ*. These criteria follow (45), (46), (47), (48), and (49).

$$RMS\quad \delta = \sqrt{\frac{1}{T}\int_0^T \delta^2(t)\,dt} \tag{45}$$

$$RMS\quad ey = \sqrt{\frac{1}{T}\int_0^T ey^2(t)\,dt} \tag{46}$$

$$RMS\quad e\phi = \sqrt{\frac{1}{T}\int_0^T e\phi^2(t)\,dt} \tag{47}$$

$$RMS\quad ay = \sqrt{\frac{1}{T}\int_0^T ay^2(t)\,dt} \tag{48}$$

$$RMS\quad \theta = \sqrt{\frac{1}{T}\int_0^T \theta^2(t)\,dt} \tag{49}$$

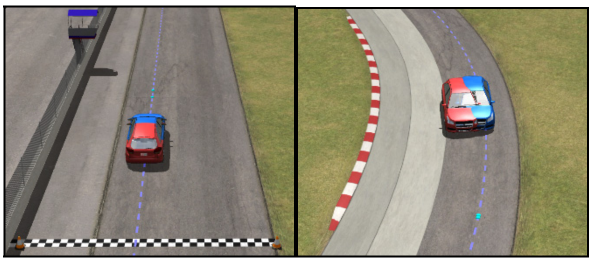

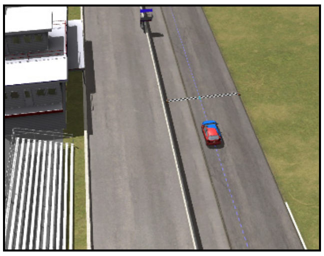

**Figure 7. Simulation's results in Carsim**

The simulation results in Carsim, shown in Figure 7, illustrate the vehicle states with the *MPC* controller (blue vehicle) and *SMC* controller (red vehicle) at the beginning, middle, and end of the trajectory. The results over the entire trajectory are presented in Figure 8, showing that the vehicle with the *MPC* controller follows the reference trajectory more closely than the vehicle with the *SMC* controller.

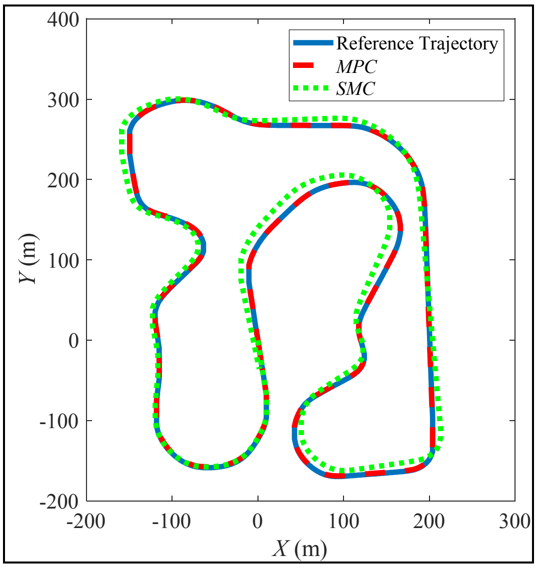


**Figure 8. Trajectories with controllers**

Corresponding to the trajectory motion in Figure 8, the braking force (pedal force) and traction force (throttle position) controlled by the *PD-FLC* are shown in Figure 9. Although the *PD-FLC* controller parameters used in both the *MPC* and *SMC* cases are identical, the responses differ. The brake pedal force in Figure 9a and throttle position in Figure 9b for the vehicle with the *MPC* controller exhibit more stable responses compared to the *SMC* controller. The timing of the maximum pedal force generated by the *PD-FLC* is the same for both *SMC* and *MPC* vehicles in the operational regions at 10 s and 60–80 s. However, there are moments when the *SMC* vehicle generates instantaneous braking forces to respond to the instantaneous speed errors of the system, such as at 30 s, 135 s, and 208 s.

Furthermore, at the same braking instant, the *SMC* vehicle exhibits a larger brake force fluctuation (148 N), which is over 36% higher than the *MPC* vehicle (110 N) at 80 s. The throttle response in Figure 9b shows that the 0% points correspond to the braking instances in Figure 9a. Over the entire operating time, the throttle responses of the *SMC* and *MPC* vehicles are nearly identical, but the *SMC* vehicle shows several larger throttle fluctu–ations at 30 s, 135 s, and 208 s. At these moments, the braking and throttle actions occur alternately; however, the fluctuation values remain low compared to the sys–tem's practical capacity, so the overall response ensures operation until the end of the trajectory. At moments of large fluctuations, the throttle response of the *SMC* vehicle is nearly six times higher than that of the *MPC* vehicle.

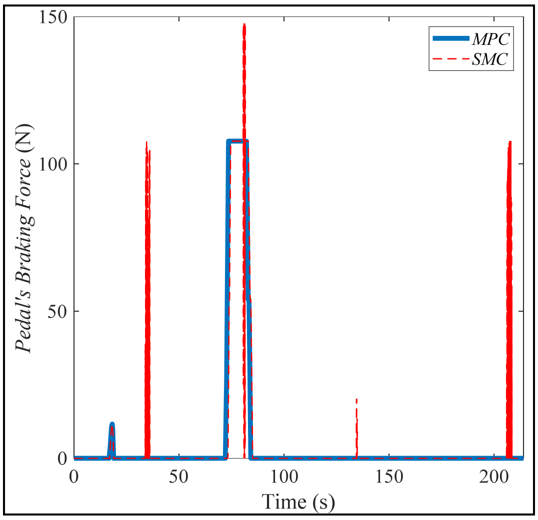


**a. Pedal's braking force**

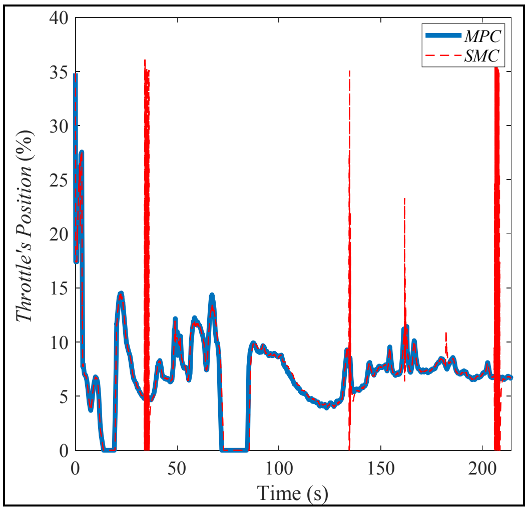


**b. Throttle's position**

**Figure 9. PD-FLC' results**

Corresponding to the trajectory in Figure 8, the ste–ering angle $\delta$, lateral acceleration $ay$, and vehicle body roll angle $\theta$ over the entire operating time for the vehicles are summarized in Figures 10, 11, and 12. Overall, throughout the operating period, the instan–taneous values of these parameters remain within the vehicle's allowable limits. Similar to the results in Figure 9, Figures 10, 11, and 12 show that the vehicle with the *SMC* controller exhibits more instances of fluc–tuations with higher amplitudes compared to the vehicle with the *MPC* controller.

Apart from the fluctuation periods, the responses of the vehicles are nearly identical. The vehicle with the *MPC* controller has a maximum steering angle below 200°, which is approximately 40% lower than that of the *SMC* vehicle (over 500°). In addition, the *MPC* ve–hicle's maximum lateral acceleration is below 0.7g, whereas the *SMC* vehicle exhibits lateral acceleration fluctuations with a peak amplitude above 0.85g. The vehicle body roll angle $\theta$ remains small (<10°), but the *MPC* vehicle shows a maximum amplitude approxi–mately 44% higher than the *SMC* vehicle.

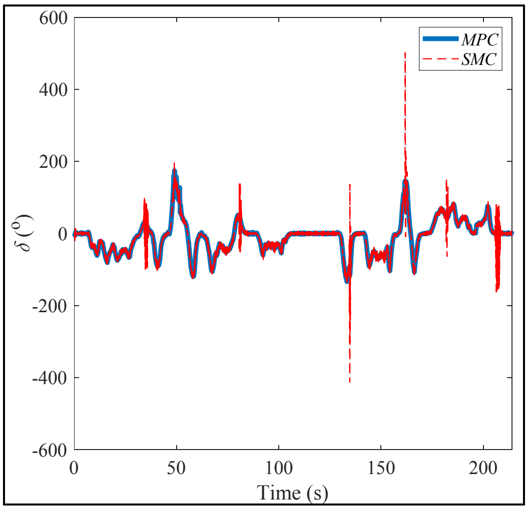


**Figure 10. Handwheel's angle**

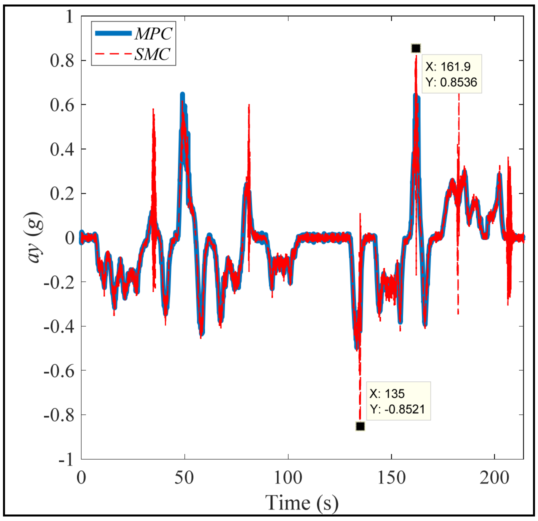


**Figure 11. Lateral acceleration**

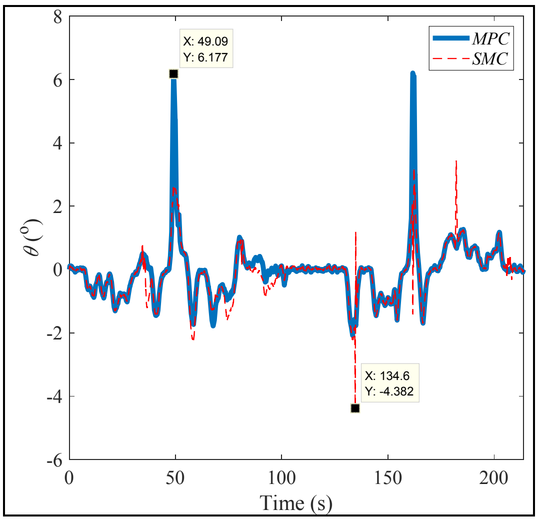


**Figure 12. Vehicle body's roll angle**

The evaluation indices of the *SMC* controller according to (43), (44), (45), and (46) are summarized and compared with the *MPC* controller in the graph of Figure 13. The results show that, on average over the entire operating trajectory, the *SMC* controller consistently exhibits higher values for $\delta$, *ay*, *ey*, and *e*□ compared to the *MPC* controller. However, the differences are small - below 5% for *RMS* $\delta$ and below 1% for *RMS ay*. The remaining indices, such as *RMS ey*, show a high difference above 15%, and *RMS e*□ nearly 10%. Only the vehicle body roll angle *RMS* $\theta$ of the *SMC* controller is lower than that of the *MPC* by 15%.

It can be observed that the vehicle with the *MPC* controller has significantly lower average errors in *ey* and *e*□ compared to the *SMC* vehicle, but exhibits considerably higher body roll responses, while the other indices show minimal differences.

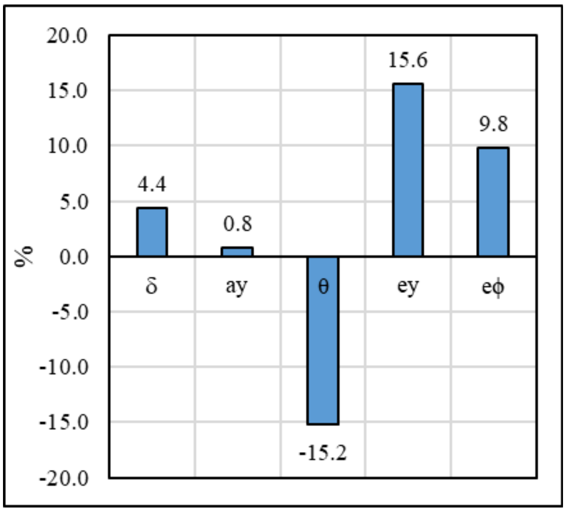


**Figure 13. Deviation rate of SMC compared to MPC**

### 5.2 Case 2

The *SMC* and *MPC* controllers, after design, are evaluated in the double-lane change scenario with simulation results in Carsim shown in Figure 14. The study assesses the performance of the controllers in Case 2 according to the criteria of maximum steering angle Max $|\delta|$, maximum distance error Max $|ey|$ maximum heading error Max $|e$□$|$, maximum lateral acceleration Max $|ay|$, and maximum vehicle body roll angle Max $|\theta|$.

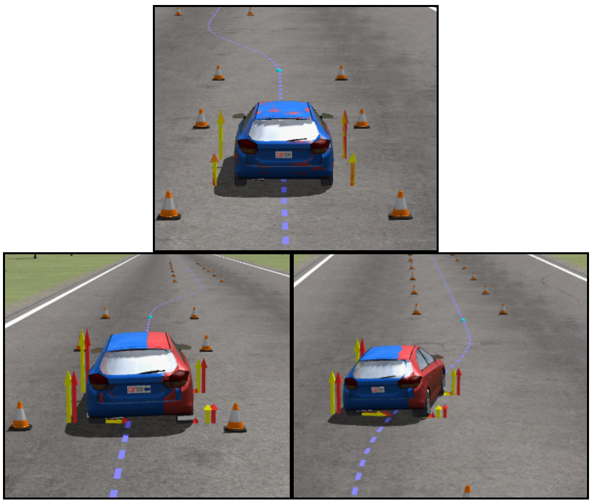

**Figure 14. Simulation's results in Carsim**

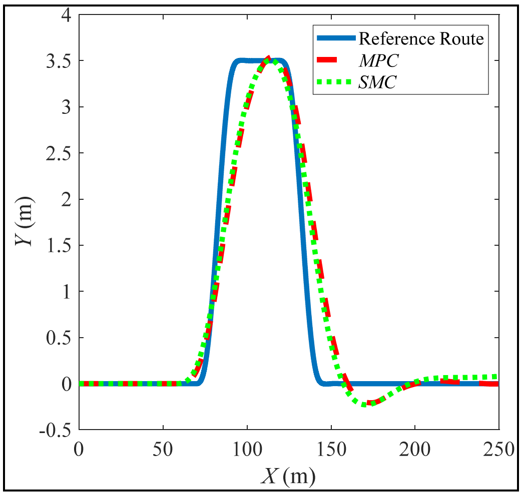


**Figure 15. Trajectories with controllers**

The results in Figure 15 show that the trajectories of the vehicles with *SMC* and *MPC* controllers are nearly identical and both satisfy the requirements for the "*Double-Lane Change*" trajectory. In the area where the trajectory merges back into the original lane, the maximum lateral deviation is below 0.25 m from the predefined *Y*-direction trajectory. Although the trajectories are similar, the steering angle responses generated by the controllers differ significantly, as shown in Figure 16. Accordingly, the *SMC* controller provides a more stable steering angle response compared to the *MPC* controller. The *MPC* controller produces $\delta$ values consistently higher than those of the *SMC* across the entire trajectory, but these $\delta$ values remain within the normal operational limits of the vehicle steering system.

Similarly, the vehicle with the *SMC* controller exhibits more stable lateral acceleration *ay* and vehicle body roll angle $\theta$, with lower peak values compared to the *MPC* controller. In this case study, the body roll angle $\theta$ is small (below 4°), while the lateral acceleration *ay* is relatively high (approximately 0.81g). Overall, the evaluation indices for both controllers in this scenario remain below the allowable limits, ensuring normal operational performance.

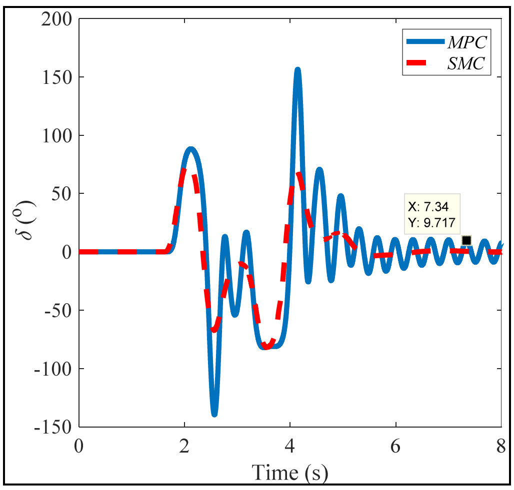


**Figure 16. Handwheel's angle**

According to the established evaluation criteria, the deviations of the *MPC* controller compared to the *SMC* controller are summarized in Figure 19.

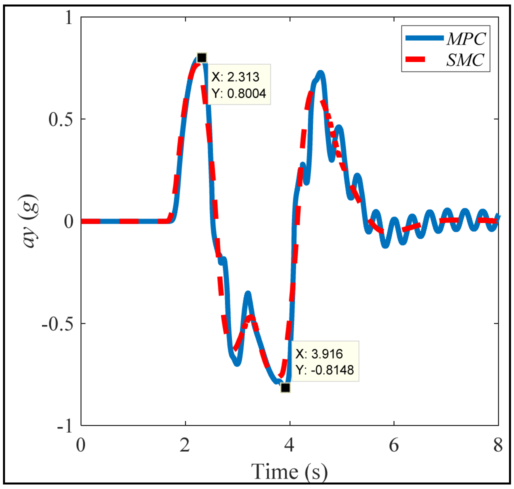


**Figure 17. Lateral acceleration**

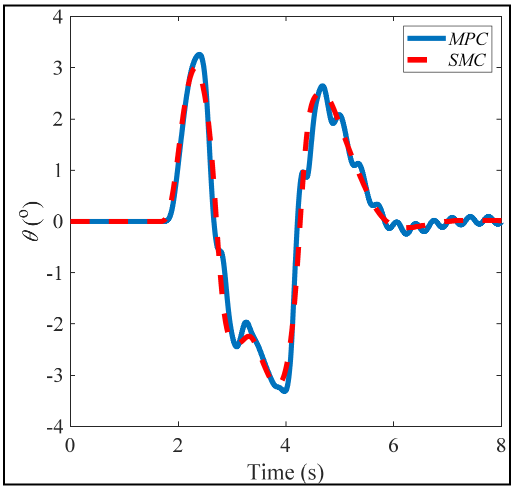


**Figure 18. Vehicle body's roll angle**

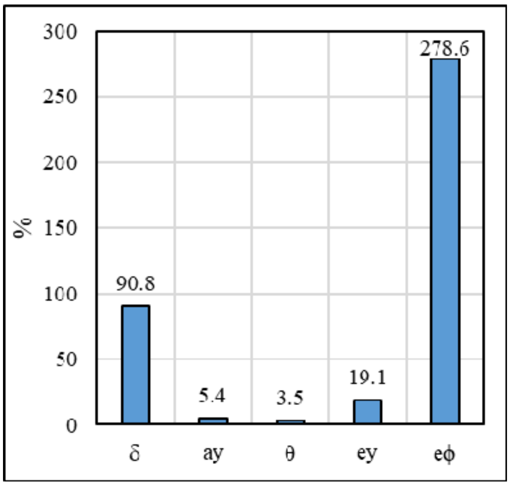


**Figure 19. Deviation rate of MPC compared to SMC**

The *SMC* controller performs better across all cri–teria. The maximum steering angle $\delta$ response of the *SMC* is 90.8% better, indicating that the *SMC* requires a smaller steering range to achieve a satisfactory trajec–tory. The heading error *e*□ response of the *SMC*, alt–hough 278% better, is not significant since this devia–tion is calculated from a small error value (below 1°). For *ay* and $\theta$, the *SMC* performs better than the *MPC*, but the improvement is minor (below 5.5%). The *SMC* produces a significantly better *ey* response compared to the *MPC*, with an improvement of nearly 20%.

## 6. CONCLUSIONS

This study applied modern controllers to manage the longitudinal and lateral motions of the vehicle, ensuring adherence to various trajectories such as "*Handling Co–urse Left Edge* – 40 km/h" and "*Double-Lane Change* – 120 km/h." A linear 3DOF dynamic model was ana–lyzed and applied to design the steering angle contro–llers. The designed controllers were then tested using Carsim software. The evaluation criteria were diverse, comprehensively reflecting different aspects of vehicle operation, including lateral stability, vehicle body roll motion, and passenger comfort. Accordingly, the main novelties and contributions of this study include:

* A complete methodology for designing the *PD-FLC* controller was established, applied to simulta–neously control the brake pedal force and throttle position to regulate the vehicle's longitudinal speed.

* A complete methodology for designing the *MPC* controller was established, involving the pre-calculation of the steering angle based on the minimization of the objective function *J*. This approach simplifies the computation of the required control input.

* A complete methodology for designing the *SMC* controller using the *Decoupled Algorithm* was established for a system in which the control input $\delta$ simultaneously appears in the dynamic equations describing the trans–lational motion along *Gy* and the rotational motion around *Gz*. Additionally, the Hurwitz condition was applied to determine the relationship among the sliding surface coefficients, ensuring rapid computation and high stability.

* A complete methodology was established for the simultaneous optimization of multiple complex parame–ters of the *PD-FLC–SMC* controllers (7 parameters) and *PD-FLC–MPC* controllers (12 parameters) using *GA*, with constraints on stability and passenger comfort according to ISO 2631:1-1997.

Simulation results show that the *MPC* controller enables the vehicle to follow the trajectory more accurately and achieve better response indices (except $\theta$), particularly with *RMS ey* improving by 15% com–pared to the *SMC* controller in "Case 1." Evaluation results for Case 2 indicate that the *SMC* controller out–performs the *MPC* in all indices, notably achieving nearly 20% better trajectory tracking with a maximum steering angle value less than 90°.

The research results can be further developed by integrating simultaneous optimization with vehicle sta–bility systems such as *ABS*, *ESC*, and *TCS* for autono–mous vehicles under various road operating conditions.

## ACKNOWLEDGEMENT

We acknowledge Ho Chi Minh City University of Tec–hnology (HCMUT), VNU-HCM for supporting this study.

## REFERENCES

[1] J Wit, C D Crane, D Armstrong. Autonomous ground vehicle path tracking. *Journal of Robotic Systems*, 2004, 21(8): 439-449.

[2] Y Wu, L Wang, J Zhang, F Li. Path following control of autonomous ground vehicle based on nonsingular terminal sliding mode and active disturbance rejection control. *IEEE Transactions on Vehicular Technology*, 2019, 68(7): 6379-6390.

[3] S Y Vural, C Hajiyev. A comparison of longitudinal controllers for autonomous UAV. *International Journal of Sustainable Aviation*, 2014, 1(1): 58-71.

[4] P E I Pounds, D R Bersak, A M Dollar. Stability of small-scale UAV helicopters and quadrotors with added payload mass under PID control. *Autonomous Robots*, 2012, 33(1-2): 129-142.

[5] J Guo, F-C Chiu, C-C Huang. Design of a sliding mode fuzzy controller for the guidance and control of an autonomous underwater vehicle. *Ocean Engineering*, 2003, 30(16): 2137-2155.

[6] Y Valeriano, A Fernandez, L Hernandez, et al. Yaw controller in sliding mode for underwater autonomous vehicle. *IEEE Latin America Transactions*, 2016, 14(3): 1213-1220.

[7] M Maurer, J C Gerdes, B Lenz, et al. *Autonomous driving*. Berlin: Springer, 2016.

[8] Y-B Lee, K-D Jang. Curved-path and velocity control of an autonomous guided vehicle using fuzzy logic. *International Journal of Computer Integrated Manufacturing*, 1998, 11(3): 255-261.

[9] N Jiang, R Qiu. Modelling and simulation of vehicle ESP system based on CarSim and Simulink. *Journal of Physics: Conference Series*, 2022, 2170(1): 012032.

[10] B Bai, G Li, H Jin, N Li, S Fallah. Research on lateral and longitudinal coordinated control of distributed driven driverless formula racing car under high-speed tracking conditions. *Journal of Advanced Transportation*, 2022, 2022: 7344044.

[11] S Sahoo, S C Subramanian, S Srivastava. Evaluation of the transient response and implementation of a heading-angle controller for an autonomous ground vehicle. *Proceedings of the Institution of Mechanical Engineers, Part D: Journal of Automobile Engineering*, 2015, 229(1): 1-17.

[12] H U Kim, T S Bae. Deep learning-based GNSS network-based real-time kinematic improvement for autonomous ground vehicle navigation. *Journal of Sensors*, 2019, 2019: 3737265.

[13] J Liu, P Jayakumar, J L Stein, T Ersal. A study on model fidelity for model predictive control-based obstacle avoidance in high-speed autonomous ground vehicles. *Vehicle System Dynamics*, 2016, 54(11): 1629-1650.

[14] Y Yuan, R Zhao. LQR-MPC-Based Trajectory-Tracking Controller of Autonomous Vehicle Subject to Coupling Effects and Driving State Uncertainties. *Sensors*, 2022, 22(15): 5556.

[15] K Yang, X Tang, Y Qin, et al. Comparative study of trajectory tracking control for automated vehicles via model predictive control and robust H-infinity state feedback control. *Chinese Journal of Mechanical Engineering*, 2021, 34(74): 1-14.

[16] A de Winter, S Baldi. Real-Life Implementation of a GPS-Based Path-Following System for an Autonomous Vehicle. *Sensors*, 2018, 18(11): 3940.

[17] P Dai, J Taghia, S Lam, et al. Integration of sliding mode based steering control and PSO based drive force control for a 4WS4WD vehicle. *Autonomous Robots*, 2018, 42(3): 553-568.

[18] R Shet, G V Lakhekar, N C Iyer. Intelligent fractional-order sliding mode control based maneuvering of an autonomous vehicle. *Journal of Ambient Intelligence and Humanized Computing*, 2024, 15(6): 2807-2826.

[19] B Ma, W Pei, Q Zhang. Trajectory tracking control of autonomous vehicles based on an improved sliding mode control scheme. *Electronics*, 2023, 12(12): 2748.

[20] F Xie, G Liang, Y-R Chien. Highly robust adaptive sliding mode trajectory tracking control of autonomous vehicles. *Sensors*, 2023, 23(7): 3454.

[21] P Hu, J Guo, L Li, et al. A robust longitudinal sliding-mode controller design for autonomous ground vehicle based on fuzzy logic. *International Journal of Vehicle Autonomous Systems*, 2013, 11(4): 368-383.

[22] J Liu, P J Jayakumar, J L Stein, et al. A nonlinear model predictive control formulation for obstacle avoidance in high-speed autonomous ground vehicles in unstructured environments. *Vehicle System Dynamics*, 2018, 56(6): 853-882.

[23] C Sun, X Zhang, Q Zhou, et al. A model predictive controller with switched tracking error for autonomous vehicle path tracking. *IEEE Access*, 2019, 7: 44507-44515.

[24] Y M Choi, J-H Park, et al. Game-based lateral and longitudinal coupling control for autonomous vehicle trajectory tracking. *IEEE Access*, 2022, 10: 31723-31731.

[25] J Hu, S Xiong, J Zha, et al. Lane Detection and Trajectory Tracking Control of Autonomous Vehicle Based on Model Predictive Control. *International Journal of Automotive Technology*, 2020, 21(2): 285-295.

[26] C Zhang, D Chu, S Liu, et al. Trajectory planning and tracking for autonomous vehicle based on state lattice and model predictive control. *IEEE Intelligent Transportation Systems Magazine*, 2019, 11(2): 29-40.

[27] F Lin, Y Chen, Y Zhao, et al. Path tracking of autonomous vehicle based on adaptive model predictive control. *International Journal of Advanced Robotic Systems*, 2019, 16(5): 1-12.

[28] C Kim, Y Yoon, S Kim, et al. Trajectory planning and control of autonomous vehicles for static vehicle avoidance in dynamic traffic environments. *IEEE Access*, 2023, 11: 5772-5788.

[29] F Yakub, A Abu, S Sarip, et al. Study of model predictive control for path-following autonomous

ground vehicle control under crosswind effect. *Journal of Control Science and Engineering*, 2016, 2016: 1-18.

[30] N E Hodge, L Z Shi, M B Trabia. A distributed fuzzy logic controller for an autonomous vehicle. *Journal of Robotic Systems*, 2004, 21(10): 499-516.

[31] V Subramanian, T F Burks, W E Dixon. Sensor fusion using fuzzy logic enhanced Kalman filter for autonomous vehicle guidance in citrus groves. *Transactions of the ASABE*, 2009, 52(5): 1411–1422.

[32] B Y Suprapto, S Dwijayanti, M I Fadillah. Design and optimization of a type-2 fuzzy logic-based late–ral control system for enhancing trajectory stabi–lity in autonomous vehicles. *Eastern-European Jo–urnal of Enterprise Technologies*, 2025, 3(3): 86–104.

[33] N Thinh, and N Phuong. A Comparative Study of 2D and 3D LiDAR Technologies in the Industrial Applications of Autonomous Navigation. *FME Transactions*, 2026, 54(1): 146-158.

[34] J Reza. *Vehicle Dynamics: Theory and Applications*. New York: Springer, 2008.

[35] T Hiep, V Thang, H Thong, et al. Control of the side brush street sweeper for various road surfaces using PID and sliding mode controllers. *FME Transactions*, 2023, 51(3): 318-328.

[36] P Dai, Genetic Algorithm Application in Multi–Objective Optimization of Structural Parameters and PID Controller Parameters on Bus Driver Seat's Suspension System. *FME Transactions*, 2025, 53(3): 426-436.

[37] W Liuping. *Model Predictive Control System Design and Implementation Using MATLAB*. UK: Springer, 2009.

[38] J Liu. *Sliding Mode Control Using MATLAB*. USA: Academic Press, 2017.

[39] ISO 2631-1. *Mechanical vibration and shock—Evaluation of human exposure to whole-body vibration—Part 1: General requirements*, 1997.

[40] M Achille. *Optimization in Practice with MATLAB for Engineering Students and Professionals*. USA: Cambridge University Press, 2015.

## NOMENCLATURE

| | | | |
|---|---|---|---|
| $l$ | Wheel base | 2.91 | m |
| $a_1$ | Distance of A and G | 1.015 | m |
| $a_2$ | Distance of B and G | 1.895 | m |
| $m$ | Vehicle mass | 1413 | kg |
| $C_{\alpha f}$ | Front cornering stiffness | 128662 | N/rad |
| $C_{\alpha r}$ | Rear cornering stiffness | 69890 | N/rad |
| $I_z$ | Yaw moment of inertia | 1536.7 | kg.m$^2$ |
| $g$ | Gravitational acceleration | 9.81 | m/s$^2$ |
| $v_x$ | Longitudinal velocity of reference model | 11.11 | m/s |
| $v$ | Vehicle velocity | -- | m/s |
| $v_f, v_r$ | Front and rear velocity at the contact patch | -- | m/s |
| $\beta$ | Vehicle's sideslip angle | -- | ° |
| $\delta$ | Front wheel's steering angle | -- | ° |
| □ | Vehicle's yaw angle | -- | ° |
| $F_{xf}$, $F_{xr}$ | Front and rear longitudinal force | -- | N |
| $F_{yf}$, $F_{yr}$ | Front and rear lateral force | -- | N |
| $\mu$ | Friction coefficient | 0.9 | -- |

## ДИЗАЈН НАВИГАЦИОНИХ СИСТЕМА ЗАСНОВАН НА ПРЕДИКТИВНОМ И КЛИЗНОМ РЕЖИМУ УПРАВЉАЊА МОДЕЛОМ ЗА ПРАЋЕЊЕ ПУТАЊЕ АУТОМОБИЛА БЕЗ ВОЗАЧА

**Н.Д. Фам**

Ова студија пројектује модерне контролере, SMC и MPC, за управљање кретањем возила како би се осигурало прецизно праћење путање жељеном брзи–ном. Уздужно кретање се регулише путем гаса и кочнице помоћу PD-FLC контролера, док се бочно кретање контролише углом управљања помоћу SMC и MPC. Новина SMC-а лежи у коришћењу раздво–јеног алгоритма, који се бави моделом где улаз уп–рављања истовремено утиче на транслациону дина–мику и ротациону динамику, што није широко при–мењено у аутономним возилима. Новина MPC-а лежи у коришћењу унапред израчунате подесиве матрице коефицијената засноване на принципу уда–љеног хоризонта, што поједностављује дизајн у поређењу са континуираном оптимизацијом током рада. Симула–ције у Matlab Simulink/Carsim под ус–ловима „Руко–вање левом ивицом курса" и „Промена двоструке траке" показале су да је у случају 1, MPC постигао боље метрике перформанси, са 15% мањом просеч–ном грешком у растојању од SMC, док је у случају 2, SMC надмашио MPC по свим метрикама, посебно у придржавању путање, са побољшањем од 20%.